**PAPER • OPEN ACCESS**

# Optimization of adsorption of methyl orange from aqueous solution by magnetic $CoFe_2O_4$/ZnAl-layered double hydroxide composite using response surface methodology

To cite this article: Yiene Molla Desalegn *et al* 2023 *Mater. Res. Express* **10** 015505

View the article online for updates and enhancements.

# Materials Research Express

# Optimization of adsorption of methyl orange from aqueous solution by magnetic CoFe$_2$O$_4$/ZnAl-layered double hydroxide composite using response surface methodology

Yiene Molla Desalegn[1,*] , Endrias Adane Bekele[2], Temesgen Abeto Amibo[3] and Temesgen Debelo Desissa[4]

1   School of Mechanical and Chemical Engineering, Department of Mechanical Engineering, Woldia Institute of Technology, Woldia University, Woldia, Ethiopia
2   Faculty of Materials Science and Engineering, Jimma Institute of Technology, Jimma University, Jimma, Ethiopia
3   Department of Process Engineering and Chemical Technology, Faculty of Chemistry, , Gdansk University of Technology, Narutowicza 11/12, 80-233 Gdansk, Poland
4   School of Mechanical, Chemical and Materials Engineering (SoMCME), Department of Materials Science and Engineering Adama Science and Technology University (ASTU), Adama, Ethiopia
*   Author to whom any correspondence should be addressed.

**E-mail:** yiene21ayl@gmail.com

## Abstract

The CoFe$_2$O$_4$/ZnAl-layered double hydroxide (LDH) composite was successfully developed through a facile co-precipitation method, characterized, and applied as an effective adsorbent for the removal of methyl orange (MO) dye from aqueous solutions. The central composite design (CCD) of the response surface methodology (RSM) was employed to estimate and optimize process variables such as initial MO concentrations, solution pH, adsorbent dosage, and contact time. 98.878% adsorption efficiency was obtained at an initial concentration of 18.747 mg l$^{-1}$ of MO, with an adsorbent dosage of 0.048 g, a solution pH of 2.770, and a contact time of 85.890 min. Analysis of variance (ANOVA) confirmed the significance of the predicted model (R$^2$ = 0.9844). Kinetic and equilibrium studies indicated that the experimental data for MO adsorption were best described by pseudo-second-order kinetic and Langmuir models. The maximum monolayer adsorption capacity of the CoFe$_2$O$_4$/ZnAl-LDH for MO was 42.3 mg g$^{-1}$.

## 1. Introduction

Dyes are widely used in several industries such as plastics, textile, paper, printing, and food industries as colorants [1]. Textile effluents contain about 15% of the total world production of dyes that is lost during the dyeing process [2]. Organic dyes from industrial effluents are commonly discharged into aqueous environments without proper treatment which caused devastating impact on human being and microorganisms. This is because of their complex aromatic molecular structure, high solubility, and low biodegradability [3, 4]. One of the organic dyes often found in industrial effluents is methyl orange (MO). MO is an anionic azo dye that poses the abnormal coloration of water bodies, hinders the penetration of Sunlight, and causes depletion of dissolved oxygen in water [5, 6]. Because of toxicity, carcinogenicity, or teratogenicity, it is considered as a major threats to living organisms and the surrounding environment [6, 7]. Therefore, it is crucial to remove dyes from contaminated water bodies before discharging into the environment using various technologies such as photocatalytic degradation, reverse osmosis, nanofiltration, flocculation, and adsorption [8]. Among the aforementioned methods, the adsorption approach has been widely applicable due to its efficiency, economic feasibility, recycling of adsorbent, and environmental friendliness [9, 10]. In recent times, adsorbents like LDH materials have gained substantial research attention by researchers.

The application of LDH materials for the adsorption of various organic dyes has been considered as a great potential for being applied in adsorption field, due to the low starting materials cost, highly positive surface

charge, easy way to prepare, high efficiency and environmentally friendly nature [11]. LDHs are known as hydrotalcite-like compounds or anionic clays, widely used in the removal of organic and inorganic pollutants [12, 13]. The LDHs are generally expressed with the general formula $[M_{1-X}^{2+}M_X^{3+}(OH)_2]^{X+}[A_{x/n}^{n-}]^{x-}.mH_2O$, where $M^{2+}$ denotes divalent cations ($Mg^{2+}$, $Ni^{2+}$, $Zn^{2+}$, $Ca^{2+}$, $Co^{2+}$ or $Cu^{2+}$), $M^{3+}$ represents trivalent cations ($Al^{3+}$, $Fe^{3+}$ or $Cr^{3+}$), and $A^{n-}$ represent an interlayer anions ($CO_3^{2-}$, $NO_3^-$ or $Cl^-$); x denoted as the molar ratio of $M^{2+}$ to total metal ions [3, 9]. The presence of a high concentration of hydroxyl groups on the surface, interlayer anion mobility of its host $A^{n-}$ and inherent positive charges make LDHs a promising adsorbent for dye adsorption from contaminated water [14–16]. However, it is tedious to separate LDHs from water as it tends to disperse due to their small particle size [17]. In this regard, combining magnetic particles with LDHs has been the solution to facilitate the recovery and separation process at the end of adsorption. Among magnetic materials, spinel cobalt ferrite ($CoFe_2O_4$), has a strong magnetic response as well as excellent chemical stability and biocompatibility [18]. Furthermore, it possesses not only high surface areas but can also bind oxy-anions [19, 20]. Earlier reports demonstrate that a composite of CuAl-LDH with $CoFe_2O_4$ nanoparticles can be generated [18] and the composite can remove a high level of anionic dye adsorption. These composites displayed a strong magnetic character arising from the small size of the magnetic nanoparticles in the composite. The objective of this study was to evaluate the efficiency of $CoFe_2O_4$/ZnAl-LDH composite for the removal of MO from an aqueous solution using the design of the experiment. The composite was characterized by X-ray diffraction (XRD), Scanning electron microscopy (SEM), Fourier transform infrared (FTIR), and Brunauer–Emmett–Teller (BET) techniques.

## 2. Materials and methods

### 2.1. Chemicals and reagents
All chemicals and reagents were used without further purification. The ferric chloride hexahydrate ($FeCl_3.6H_2O$, 99%), cobalt nitrate hexahydrate ($Co(NO_3)_2.6H_2O$, 97%), aluminum nitrate ($Al(NO_3)_3.9H_2O$, 99% ), Zinc nitrate hexahydrate $Zn(NO_3)_2.6H_2O$, sodium carbonate ($Na_2CO_3$, 99%), sodium hydroxide (NaOH), hydrochloric acid (HCl), ethanol ($C2H_5OH$, 99.9%) and methyl orange (MO) were used in the experimental work.

### 2.2. Synthesis of $CoFe_2O_4$
$CoFe_2O_4$ was synthesized according to our previous work with slight modifications [10]. First, to prepare 2 g of $CoFe_2O_4$, about 4.611 g $FeCl_3.6H_2O$ and 2.483 g of $Co(NO_3)_2.6H_2O$ were dissolved in 100 ml distilled water for about 15 min, forming a homogeneous solution. To this was then added a solution of 2M NaOH until pH 11. Then, the mixture was stirred for a further 3 h at 70 °C in a constant temperature heating water bath. After that, a suspension was formed and the solid precipitate was collected and washed by solvents such as distilled water and ethanol several times until neutral supernatant is found. Finally, the product was dried at 100 °C overnight.

### 2.3. Synthesis of ZnAl-LDH
ZnAl-LDH with a molar ratio of Zn to Al (3:1) was prepared by a co-precipitation method [21]. Typically, 22.5 mmol of $Zn(NO_3)_2 \cdot 6H_2O$ and 7.5 mmol of $Al(NO_3)_2 \cdot 9H_2O$ were dissolved in 150 ml distilled water (solution A). Separately, an aqueous solution containing 1.2 M $Na_2CO_3$ and 0.6 M NaOH in 100 ml distilled water (solution B) was prepared. Then, Solution B was added dropwise into solution A under vigorous stirring until the slurry's final pH becomes 10. The slurry was aged at 65 °C for 24 h and washed several times with distilled water and ethanol to remove excess soluble ions, until the filtrate pH was close to 7. Finally, the as-synthesized precipitate was dried at 70 °C for 20 h, and ZnAl-LDH powder was obtained.

### 2.4. Synthesis of $CoFe_2O_4$-ZnAl LDH composite
A facile co-precipitation method was employed for the preparation of the magnetic $CoFe_2O_4$/ZnAl-LDH composite. To obtain a uniform suspension, the as-prepared $CoFe_2O_4$ (0.5 g) was ultrasonically dispersed into 150 ml doubly distilled water for 30 min in a 500 ml beaker for 15 min to obtain a uniform suspension, and the precipitate formed will be then stirred vigorously at 60 °C. Whilst, adding dropwise solution (100ml) containing 0.125 mol $L^{-1}$ (4.689) $Al(NO_3)_3.9H_2O$ and 0.25 mol $l^{-1}$ (6.41 g) $Mg(NO_3)_2.6H_2O$. Then the pH was adjusted to 10 by adding a 100 ml alkaline solution containing 3.375 g NaOH and 2.645 g $Na_2CO_3$. Then the precipitate was left to age for 8 h at 60 °C. After that, the product was washed with doubly distilled water until the pH of the supernatant was neutral. The resulting sample was dried at 100 °C overnight.

**Table 1.** Levels of the adsorption process parameters considered.

| Variables | Variable coding | Units | -alpha | Low | Center point | High | +alpha |
|---|---|---|---|---|---|---|---|
| Initial MO concentration | A | $mg\,l^{-1}$ | 10 | 15 | 20 | 25 | 30 |
| pH | B | — | 2 | 2.5 | 3 | 3.5 | 4 |
| Adsorbent dosage | C | $g\,l^{-1}$ | 0.4 | 0.7 | 1 | 1.3 | 1.6 |
| Contact time | D | min | 25 | 50 | 75 | 100 | 125 |

## 2.5. Materials characterizations

X-ray powder diffraction (XRD-7000, Drawell, China) was used to characterize the crystalline composition of the as-synthesized adsorbents. The morphology was determined by scanning electron microscope (JEOL/EO, JSM-6000 plus). Fourier transform infrared spectroscopy (FTIR, PerkinElmer) was used to identify functional groups from a wave number of 500–4000 $cm^{-1}$ at a resolution of 4. The textural properties of the prepared $CoFe_2O_4/ZnAl$-LDH which include BET surface area, pore volume, and pore size distributions were determined using a Quantachrome analyzer (Nova station C, version 11.0, USA) based on the principle of adsorption/desorption of nitrogen at 77.3 K and 60/60 s (ads/des) equilibrium time.

## 2.6. Experimental design and statistical analysis

In this study, the CCD of RSM was employed to optimize the processing variables estimating the regression model equation [22, 23]. RSM can be used to evaluate the effects of individual variables, the interaction of variables, and the optimum conditions for responses [24]. Four process independent variables were chosen: initial MO concentration, solution pH, adsorbent dosage, and contact time, and their effects on the response were estimated. The total number of experiments can be determined from the following equation:

$$N = 2^n + 2n + n_c \tag{1}$$

Where N is the total number of experiments required, n is the number of factors and $n_c$ is the center point. Since a total of 30 experimental runs were conducted in this work, $2^4 = 16$ cube points, 6 replications at the center point and 8 axial points. The level of chosen input variables and experimental ranges for MO removal efficiency (R) are presented in table 1. The response variable ($\eta$) can be expressed as a function of the independent process Variables, according to the following quadratic model:

$$\eta = a_0 + \sum_{j=1}^{4} a_j Y_j + \sum_{j=1}^{4} a_{jj} Y_j^2 + \sum_{I}\sum_{<j=2}^{4} a_{ji} Y_i Y_j + e_i \tag{2}$$

Where $\eta$ is the response, $Y_i$ and $Y_j$ refer to variables (i and j range from 1 to k); $a_0$ refers to the coefficient of intercept; $a_j$, $a_{jj}$, and $a_{ij}$ are known to be coefficients of interaction for the variables, respectively; and $e_i$ is the error.

 The obtained experimental data were analyzed using Design expert 13.0 software, and the significance of the developed model was tested using analysis of variance (ANOVA). The interactions between the independent variables and their effect on the response variable were studied systematically through the response surface contour plots.

## 2.7. Batch adsorption studies.

The MO removal experiment was conducted in a set of each 250 ml conical flasks containing 50 ml of the required concentration of an adjusted pH of MO solution. Solution pH was varied from 2–4 by adding HCl solution. Then, the required amount of the composite was added to the solution and stirred for a particular period of time. The composite was separated from the MO solution through centrifugation (750 rpm) for 10 min. The concentration of the dye solution was then analyzed for absorbance using JASCO UV–vis spectrometer at maximum absorbance ($\lambda_{max} = 464$ nm). For the sake of comparison, blank experiments were conducted in parallel on MO solutions, without the addition of an adsorbent. All tests were carried out in triplicate, and their mean values were used in analyzing the data.

 The MO removal efficiency, $\eta$ (%) was calculated using the following equation [25].

$$\% = \frac{(C_o - C_t)}{C_o} \times 100 \tag{3}$$

The adsorption capacity of the materials can be calculated according to equation (4) below [26]:

$$q_e = \frac{(C_o - C_t)V}{m} \tag{4}$$

Where $C_o$ and $C_e$ is the initial and equilibrium concentration of MO ($mg\,l^{-1}$), $V$ is the solution volume (L), and $m$ is the adsorbent dosage (g). All experiments were performed in triplicate, and the mean value was reported.
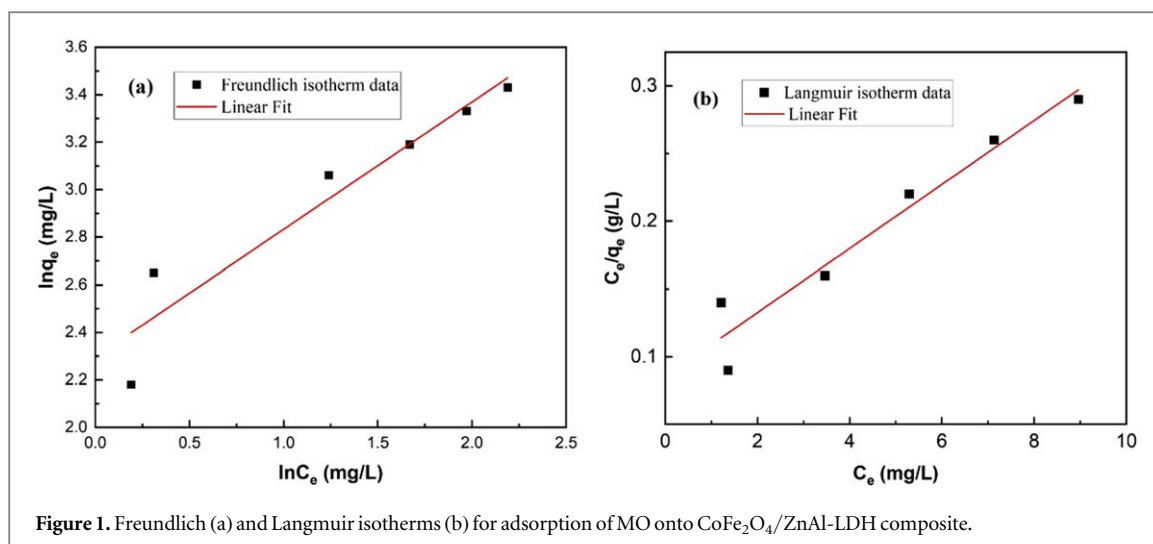
**Figure 1.** Freundlich (a) and Langmuir isotherms (b) for adsorption of MO onto CoFe$_2$O$_4$/ZnAl-LDH composite.

**Table 2.** Parameters of Freundlich and Langmuir isotherms for adsorption of MO onto CoFe$_2$O$_4$/ZnAl-LDH.

| Isotherm models | Parameters | Values | $R^2$ |
|---|---|---|---|
| Freundlich | $n$ | 1.8661 | 0.9158 |
| | $K_F (L\,g)^{-1}$ | 9.9466 | |
| Langmuir | $q_{max} (mg\,g)^{-1}$ | 42.30 | 0.9428 |
| | $b (1\,mg)^{-1}$ | 0.2769 | |
| | $R_L$ | 0.0828 | |

## 2.8. Adsorption isotherm analysis

In this study, Freundlich and Langmuir adsorption isotherms were used to study the adsorption mechanism [10].

The Freundlich isotherm assumes a monolayer adsorption process with heterogeneous surfaces [27] and this process further assumes that there is an interaction of adsorbed species [28]. The equation describing this model can be given as in equation (5) below [28]:

$$\ln q_e = \ln K_f + \frac{1}{n}\ln C_e \tag{5}$$

Where $K_F$ is the Freundlich constant which represents the affinity of the adsorbent towards adsorbet and $1/n$ is an adsorption intensity that varies with the heterogeneity of the adsorbed monolayer on adsorbing surfaces.

The Langmuir isotherm model assumes that the adsorption occurs on homogeneous surfaces without interaction between the adsorbed MO [29], and can be expressed according to the following equation (6) below [28].

$$\frac{C_e}{q_e} = \frac{1}{q_{max}\,b} + \frac{1}{q_{max}}C_e \tag{6}$$

Where $b\,(1\,mg)^{-1}$ is the Langmuir adsorption constant and $q_{max}$ is the maximum adsorption capacity of the adsorbent (mg g$^{-1}$). The fitting isotherm and calculated parameters for freundlich and langmuir adsorption were presented in figure 1 and table 2.

Furthermore, the favorability of Langmuir isotherm can be described by separation factor ($R_L$) whether it is favorable ( $0 < RL < 1$ ), unfavorable ( $RL > 1$ ), irreversible ( $RL = 0$ ) or linear ( $RL = 1$ ) as described in the following equation (7):

$$R_L = \frac{1}{1 + bC_o} \tag{7}$$

where $Co$ (mg l$^{-1}$) is the maximum initial MO concentration and $b$ (L mg)$^{-1}$ is the Langmuir equilibrium constant [30].

## 2.9. Kinetic modeling

The kinetics of adsorption describes the rate of dye uptake by adsorbent [31]. In adsorption studies, two kinetic models are commonly used. These are pseudo-first and pseudo-second-order adsorption kinetics [32]. These

**Figure 2.** XRD pattern of (a) CoFe$_2$O$_4$, (b) ZnAl-LDH (c) CoFe$_2$O$_4$/ZnAl-LDH.
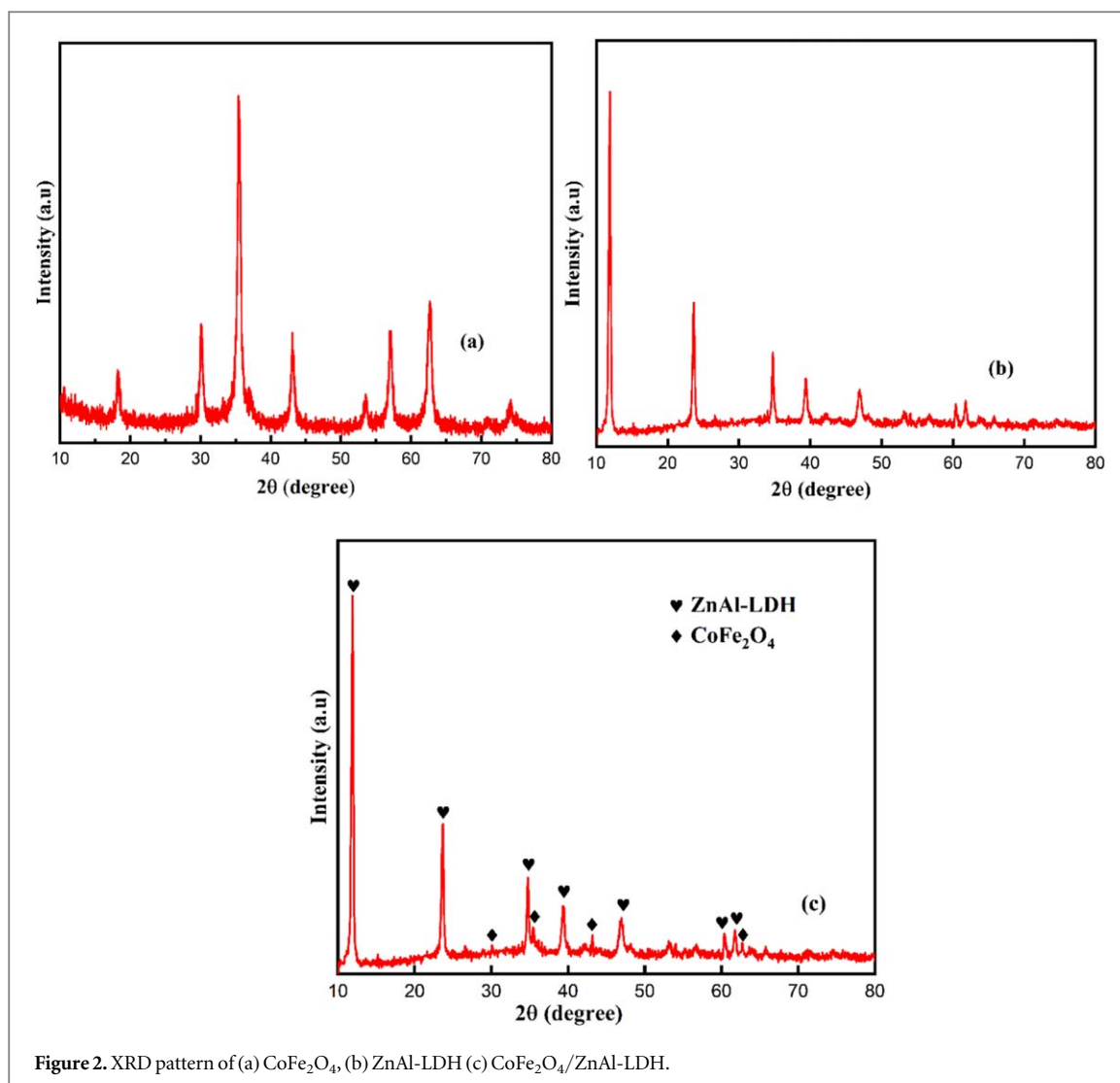
models for the present composite materials can be calculated using equations (8) and (9), respectively, as given below [26, 33–35]:

$$\log(q_e - q_t) = \log q_e - \frac{K_1}{2.303}t \tag{8}$$

$$\frac{t}{q_t} = \frac{1}{K_2 q_e^2} + \frac{1}{q_e}t \tag{9}$$

Where, $q_t$ (mg g)$^{-1}$ is the adsorption capacity at an adsorption time of $t$, and $K_1$ (1 min)$^{-1}$ and K$_2$ (g/(mg·min)) are the rate constants of pseudo-first-order and pseudo-second-order models, respectively.

# 3. Results and discussions

### 3.1. XRD analysis

Figures 2(a)–(c) shows XRD patterns of CoFe$_2$O$_4$, ZnAl-LDH and CoFe$_2$O$_4$/ZnAl-LDH samples, respectively. In figure 2(c), the appearance of diffraction peaks at $2\theta = 11.92°$, $23.68°$, $34.75°$, $39.37°$, $46.93°$, $60.37°$ and $61.75°$ were attributed to (003), (006), (009), (015), (018), (110) and (113) planes of the typical well-crystalized hydrotalcite-like LDH materials present in the composite (JCPDS no. 38–0486) [36]. These peaks are the same as those observed in figure 2(b). Particularly, the peaks at $11.92°$ correspond to carbonate ($CO_3^{2-}$) intercalated in the LDH which is resulted from Na$_2$CO$_3$ during synthesis [37].

The diffraction peaks at a 2θ of $30°$, $35.41°$, $43.15°$, and $62.68°$ corresponding, respectively, to the (220), (311), (400), (440), confirmed the incorporation of CoFe$_2$O$_4$ particles in the composite (JCPD No.22–1086) [38]. Similar peaks can be observed for pristine CoFe$_2$O$_4$ particles. Figure 2(a) shows the XRD pattern of CoFe$_2$O$_4$. The CoFe$_2$O$_4$ synthesized in this work showed high crystallinity with a space group of *Fd-3m* and a
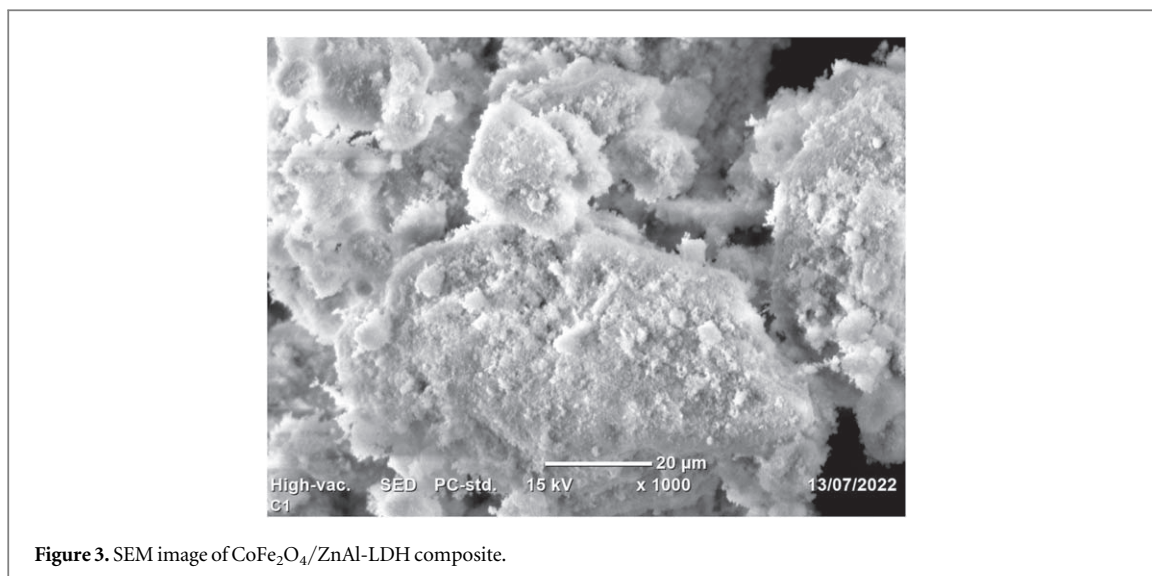
**Figure 3.** SEM image of $CoFe_2O_4$/ZnAl-LDH composite.



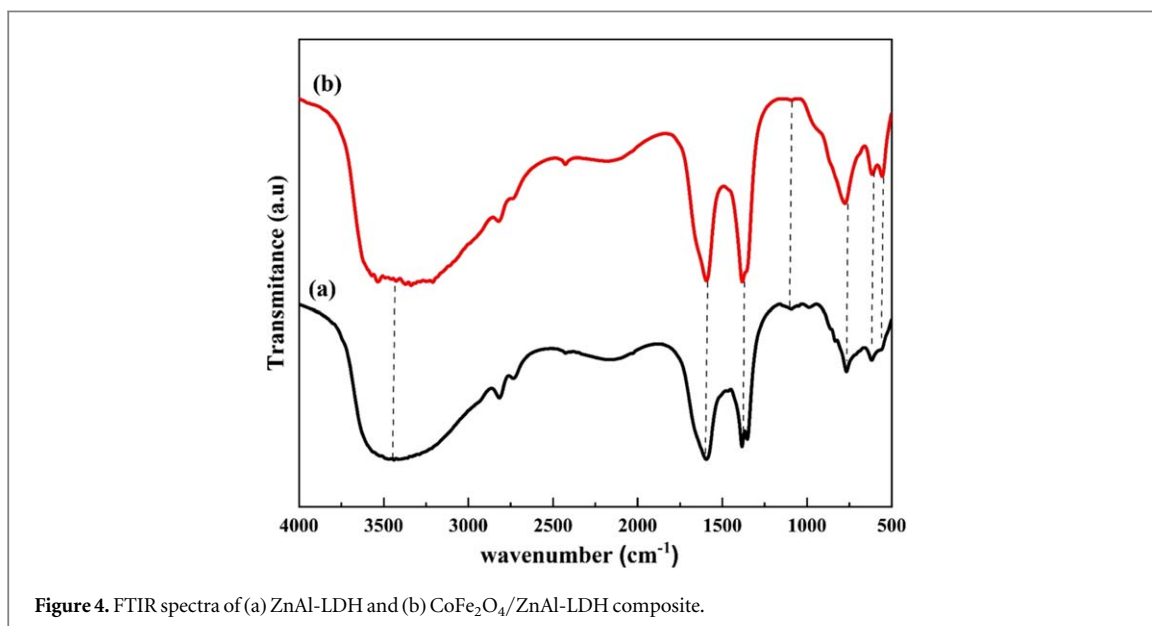**Figure 4.** FTIR spectra of (a) ZnAl-LDH and (b) $CoFe_2O_4$/ZnAl-LDH composite.

crystallographic density of 5.27 g·cm$^{-3}$, which is in an agreement to the theoretical density of about 5.29 g·cm$^{-3}$ [39]. Details of the crystallographic planes and the corresponding (hkl) of the planes are reported elsewhere [10].

### 3.2. SEM analysis

The prepared magnetic $CoFe_2O_4$/ZnAl-LDH was characterized by a scanning electron microscope (SEM) to examine the morphological properties (figure 3). $CoFe_2O_4$/ZnAl-LDH composite shows uneven particle distribution, which revealed that various agglomeration of $CoFe_2O_4$ particles were loaded on the surface of ZnAl-LDH [40]. Moreover, the surface morphology of $CoFe_2O_4$/ZnAl-LDH is rough. Because of the loading of $CoFe_2O_4$ on ZnAl-LDH, the original layered-structure of ZnAl-LDH was changed with inhomogeneous distribution of $CoFe_2O_4$ particle [10].

### 3.3. FTIR analysis

The FTIR spectra of the ZnAl-LDH and $CoFe_2O_4$/ZnAl-LDH composite are depicted in figure 4(a) and (b). The FTIR spectrum of the CoFe2O4/ZnAl-LDH composite illustrated in figure 4(b) was almost identical to that of the ZnAl-LDH. The strongest broad adsorption band at around 3444 cm$^{-1}$ is ascribed to OH− groups as reported in another study [41]. The symmetry vibration band observed at 1640 cm−1 was attributed to the interlayer water molecule. The peak at 1376 cm$^{-1}$ is showed the vibration mode of CO3$^{2-}$ [15]. The lower band frequencies between 500 and 1000 cm$^{-1}$ correspond to lattice vibration of metal-oxygen bonding to the layers of the LDH and $CoFe_2O_4$ [41]. The vibration modes of the carbonate anions were also illustrated at 1103 cm$^{-1}$

absorption peaks [37] . The presence of such vibration reveals the intercalation of carbonate ions into the interlayer space of ZnAl-LDH.

### 3.4. BET analysis

The typical $CoFe_2O_4$/ZnAl LDH composite presented a surface area of 499.345 $m^2\,g^{-1}$, total pore volume of 0.09321 c.c./g, and pore diameter of 1.27 nm and was characterized as a microporous material. The large active surface functionalities and high surface area with high pore volume are crucial for a good adsorbent. It is revealed that the incorporation of $CoFe_2O_4$ into the composite decreased the surface area, possibly by blocking available sites.

### 3.5. Central composite design (CCD) model and data analysis

Input variables such as MO initial concentrations, solution pH, adsorbent dosage and contact time were varied according to the design as indicated by the Design Expert Software 13. The experimental and predicted percentage removal of MO onto $CoFe_2O_4$/ZnAl-LDH adsorbent at different operating conditions were tabulated as shown below.

As suggested by the CCD, a quadratic model was chosen to represent MO removal efficiency by $CoFe_2O_4$/ZnAl-LDH composite. The second-order polynomial equation in terms of coded factors after eliminating the insignificant model terms was expressed as follows

$$
\begin{aligned}
\eta = 98 &- 1.78A - 1.40B - 0.5396C \\
&+ 1.42D - 0.4419AB - 0.9869AC \\
&- 1.06BD - 0.5156CD - 3.06A^2 \\
&- 1.95B^2 - 2.79C^2 - 2.31D^2
\end{aligned}
\tag{10}
$$

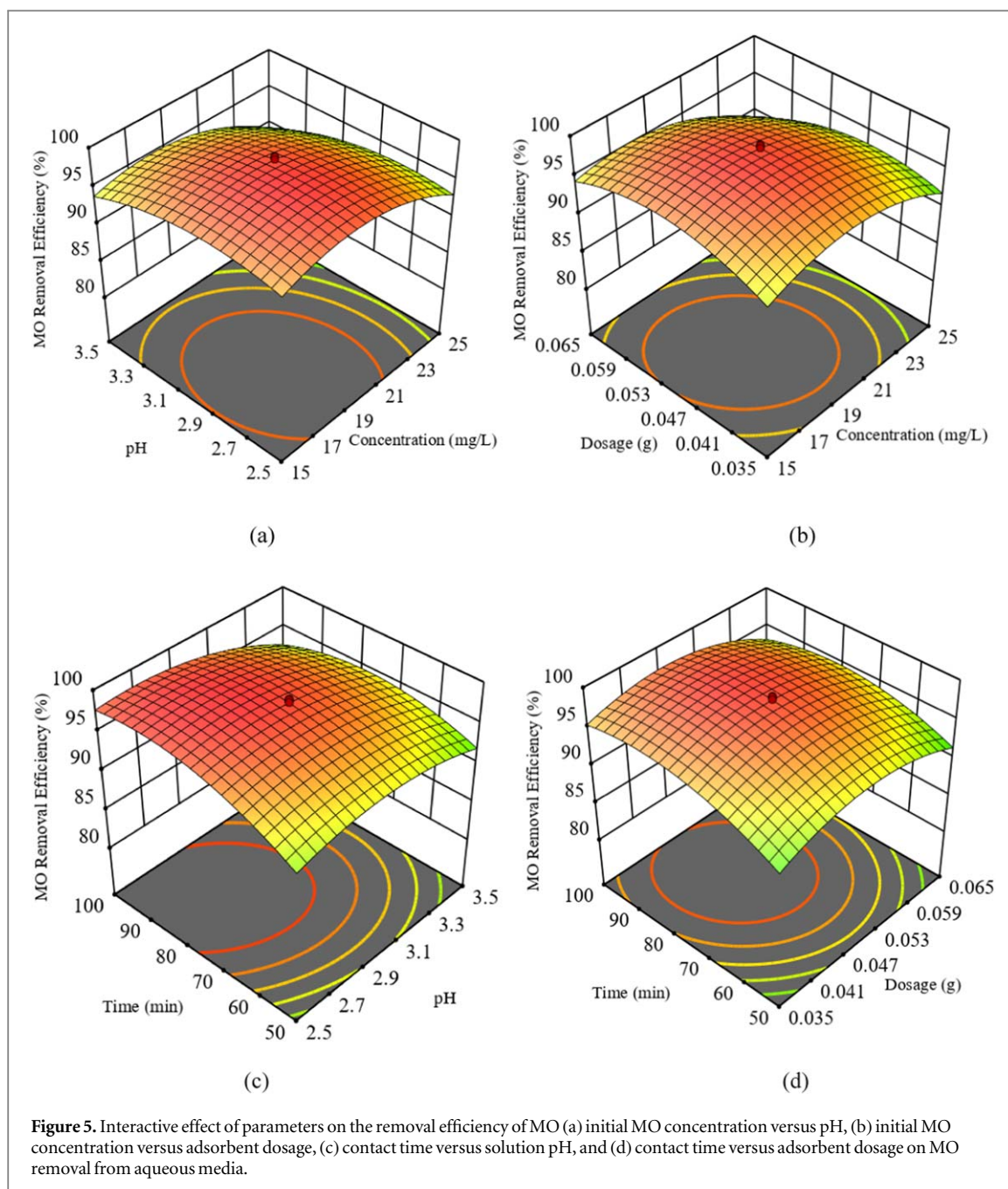where $\eta$ is the removal efficiency of MO (%), A is the concentration, B is the pH, C is the dosage of the adsorbent and D is the contact time. According to the coded quadratic equation (10), most of the parameters have negative coefficients which mean they attained their optimum value; further addition of these parameters would decrease the removal efficiency of the adsorbent. The removal efficiencies (%) of MO have been estimated by equation (3) and are presented in table 3. In general, there were agreements between the experimental and predicted values of MO removal efficiency. Furthermore, analysis of variance (ANOVA) was applied to check the statistical significance of the quadratic model (table 4). A model is said to be a good predictor of the experimental data, if $F$-value obtained is evidently greater than the tabulated $F$-value [30]. It was found that the regression was statistically significant at the F-value was 67.64 and the values of prob>F ($<0.0001$). However, values of Prob $> F$ less than 0.0500 indicate terms are significant. The lack of fit $F$-value of 0.2985 indicates the lack of fit is not significant relative to the pure error. The statistical parameters, viz. $R^2$, $R^2_{Adj}$ and $R^2_{Pred}$ were obtained as 0.9844, 0.9699 and 0.9257, respectively. 'Adeq Precision' gives the ratio of the signal to the noise. A ratio greater than 4 is desirable. Thus, the Adeq precision of 25.3891 indicates an adequate signal.

*3.5.1. Interaction effect analysis of the parameters*

A 3D representation of the adsorption of MO is shown in figures 5(a)–(d). Figure 5(a) explains the 3D surface plot of MO removal efficiency as a function of initial concentration and a solution PH at the mean of contact time and adsorbent dosage. The removal efficiency was increased by decreasing the pH of the solution and obtaining the highest removal efficiency of the adsorbent at a pH of 3. The reason for this observation could be due to an increase in electrostatic attraction between the negatively charged dye molecule and the positively charged $CoFe_2O_4$/ZnAl-LDH surface [18]. On the contrary, in a basic medium, anionic MO and $OH^-$ ions compete for the positively charged binding sites on the adsorbent surface, which leads to decreased adsorption capacity. It can also be understood that the adsorbent efficiency rises with an increase in the initial MO concentration till it reaches 20 $mg\,l^{-1}$. The interactive effect on the $CoFe_2O_4$/ZnAl-LDH adsorption towards MO dye was significant with the $p$- value of 0.0631.

Figure 5(b) depicts the 3D surface plot showing the combined effects of initial concentration and adsorbent dosage on the removal efficiency of MO. From the plot, it was observed that the removal efficiency increased with an increase in adsorbent dosage from 0.02 to 0.05 g/50 ml. This can be attributed to the high specific surface area of the composite and the availability of more active sites of $CoFe_2O_4$/ZnAl-LDH composite.

Figure 5(c) demonstrates the interaction effect of the pH of the solution and contact time on the removal of MO via $CoFe_2O_4$/ZnAl-LDH. It is obvious that the removal percentage of MO from aqueous solution increases rapidly in the initial stages and became slower in the later stages until the attainment of equilibrium (75 min) and then decreases gradually. The probable reason could be at the initial period of adsorption, the rate of MO binding with the surface of $CoFe_2O_4$/ZnAl-LDH is great due to the availability of an abundance of adsorption sites, and then MO adsorption becomes slow. This is because of the diffusion of MO into the adsorbent pores [19]. The interaction effect has a significant effect on its MO adsorption with a $p$ value of 0.0002 (table 4). The

**Figure 5.** Interactive effect of parameters on the removal efficiency of MO (a) initial MO concentration versus pH, (b) initial MO concentration versus adsorbent dosage, (c) contact time versus solution pH, and (d) contact time versus adsorbent dosage on MO removal from aqueous media.

highest removal efficacy of MO is attained at a $CoFe_2O_4/ZnAl$-LDH dosage of 0.05g/50 ml and a contact time of 75 min.

The interactive effect of adsorbent dosage and contact time is illustrated through the 3D plots as shown in figure 5(d). The removal efficiency of the adsorbent increased with an increase in the adsorbent dosage and contact time. The interaction of adsorbent dosage and contact time has a significant effect on its MO removal with a *p* value of 0.0334 (table 4). Meanwhile, it was revealed by the result obtained that contact time highly interacts with other variables.

*3.5.2. Process optimization*
The optimum values of the process parameters for the maximum MO removal efficiency were determined as shown in table 5 below. The experimental (actual) removal efficiency of $CoFe_2O_4/ZnAl$-LDH at those optimal condition was in proximate to the predicted value. This proves that the adopted method to optimize process parameters for maximum adsorption of MO onto $CoFe_2O_4/ZnAl$-LDH composite is successful.

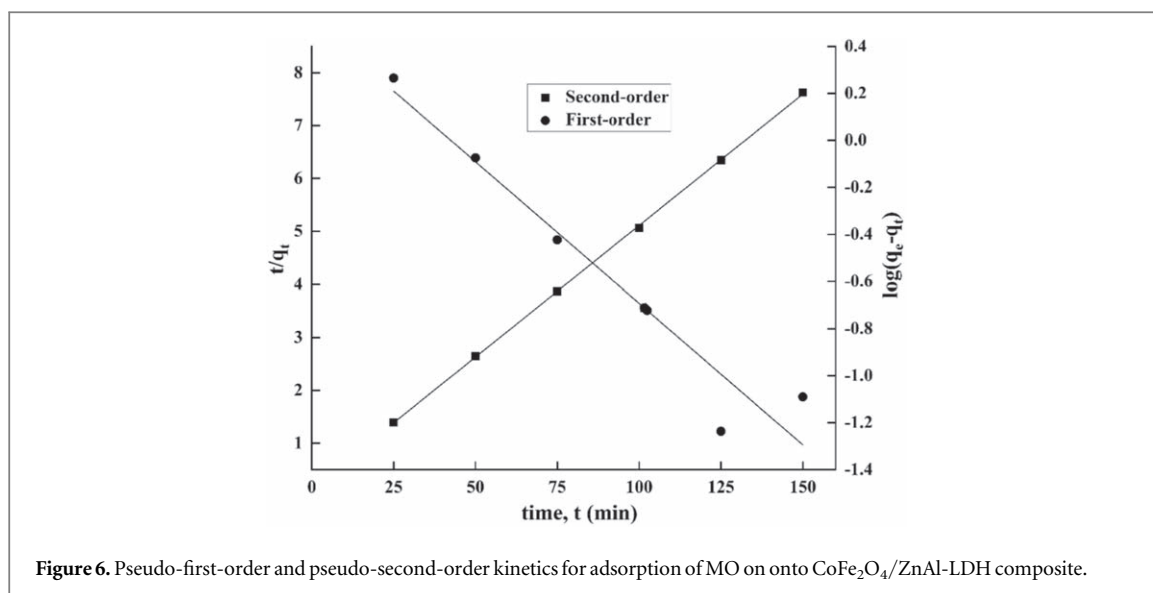**Figure 6.** Pseudo-first-order and pseudo-second-order kinetics for adsorption of MO on onto CoFe$_2$O$_4$/ZnAl-LDH composite.

**Table 3.** Batch mode adsorption process parameters used in RSM with the equivalent experimental and predicted values for response.

| Independent variables MO removal efficiency (%, $\eta$) | | | | | | | |
|---|---|---|---|---|---|---|---|
| Std | Run | A | B | C | D | Experimental | predicted |
| 23 | 1 | 20 | 3 | 0.05 | 25 | 85.58 | 85.93 |
| 11 | 2 | 15 | 3.5 | 0.035 | 100 | 88.26 | 89.04 |
| 25 | 3 | 20 | 3 | 0.05 | 75 | 98.48 | 98.00 |
| 18 | 4 | 30 | 3 | 0.05 | 75 | 82.49 | 82.20 |
| 24 | 5 | 20 | 3 | 0.05 | 125 | 92.99 | 91.59 |
| 17 | 6 | 10 | 3 | 0.05 | 75 | 90.08 | 89.32 |
| 5 | 7 | 15 | 2.5 | 0.065 | 50 | 88.17 | 88.72 |
| 7 | 8 | 15 | 3.5 | 0.065 | 50 | 89.95 | 89.43 |
| 14 | 9 | 25 | 2.5 | 0.065 | 100 | 86.99 | 87.99 |
| 20 | 10 | 20 | 4 | 0.05 | 75 | 87.68 | 87.42 |
| 19 | 11 | 20 | 2 | 0.05 | 75 | 93.81 | 93.01 |
| 12 | 12 | 25 | 3.5 | 0.035 | 100 | 85.88 | 86.27 |
| 9 | 13 | 15 | 2.5 | 0.035 | 100 | 93.06 | 93.58 |
| 15 | 14 | 15 | 3.5 | 0.065 | 100 | 88.6 | 89.41 |
| 21 | 15 | 20 | 3 | 0.02 | 75 | 88.86 | 87.94 |
| 22 | 16 | 20 | 3 | 0.08 | 75 | 85.91 | 85.78 |
| 10 | 17 | 25 | 2.5 | 0.035 | 100 | 91.94 | 92.57 |
| 3 | 18 | 15 | 3.5 | 0.035 | 50 | 87.06 | 87.00 |
| 29 | 19 | 20 | 3 | 0.05 | 75 | 98.41 | 98.00 |
| 13 | 20 | 15 | 2.5 | 0.065 | 100 | 92.88 | 92.94 |
| 8 | 21 | 25 | 3.5 | 0.065 | 50 | 82.89 | 83.31 |
| 2 | 22 | 25 | 2.5 | 0.035 | 50 | 86.76 | 86.89 |
| 1 | 23 | 15 | 2.5 | 0.035 | 50 | 86.85 | 87.29 |
| 26 | 24 | 20 | 3 | 0.05 | 75 | 98.34 | 98.00 |
| 30 | 25 | 20 | 3 | 0.05 | 75 | 98.05 | 98.00 |
| 6 | 26 | 25 | 2.5 | 0.065 | 50 | 85.03 | 84.36 |
| 4 | 27 | 25 | 3.5 | 0.035 | 50 | 84.77 | 84.83 |
| 27 | 28 | 20 | 3 | 0.05 | 75 | 98.19 | 98.00 |
| 16 | 29 | 25 | 3.5 | 0.065 | 100 | 83.02 | 82.69 |
| 28 | 30 | 20 | 3 | 0.05 | 75 | 96.54 | 98.00 |

*A* is initial MO concentration (mg l)$^{-1}$, *B* is pH, C is adsorbent dose (g/50 ml), and *D* is contact time (min).

### 3.5.3. Adsorption equilibrium isotherm

In testing the applicability of Langmuir and Freundlich isotherms, a solution of 50 ml volume containing the concentration of 10 to 40 mg l$^{-1}$ M$^{-1}$O$^{-1}$ at an adsorbent dosage of 0.047 g, pH 2.75 with the stirring speed of

**Table 4.** Analysis of variance (ANOVA) for fit of MO removal efficiency from central composite design.

| Source | Sum of squares | df | Mean square | F-value | p-value | Remark |
|---|---|---|---|---|---|---|
| Model | 734.01 | 14 | 52.43 | 67.64 | < 0.0001 | significant |
| A | 76.08 | 1 | 76.08 | 98.14 | < 0.0001 | |
| B | 46.79 | 1 | 46.79 | 60.36 | < 0.0001 | |
| C | 6.99 | 1 | 6.99 | 9.01 | 0.0089 | |
| D | 48.08 | 1 | 48.08 | 62.03 | < 0.0001 | |
| AB | 3.12 | 1 | 3.12 | 4.03 | 0.0631 | |
| AC | 15.58 | 1 | 15.58 | 20.10 | 0.0004 | |
| AD | 0.3570 | 1 | 0.3570 | 0.4606 | 0.5077 | |
| BC | 1.02 | 1 | 1.02 | 1.31 | 0.2704 | |
| BD | 18.00 | 1 | 18.00 | 23.22 | 0.0002 | |
| CD | 4.25 | 1 | 4.25 | 5.49 | 0.0334 | |
| $A^2$ | 257.06 | 1 | 257.06 | 331.62 | < 0.0001 | |
| $B^2$ | 103.91 | 1 | 103.91 | 134.05 | < 0.0001 | |
| $C^2$ | 212.95 | 1 | 212.95 | 274.72 | < 0.0001 | |
| $D^2$ | 146.53 | 1 | 146.53 | 189.04 | < 0.0001 | |
| Residual | 11.63 | 15 | 0.7752 | | | |
| Lack of Fit | 8.94 | 10 | 0.8943 | 1.67 | 0.2985 | not significant |
| Pure Error | 2.68 | 5 | 0.5369 | | | |
| Cor Total | 745.63 | 29 | | | | |

**Table 5.** Optimal conditions of the selected factors for MO adsorption via $CoFe_2O_4$/ZnAl-LDH.

| Optimized process parameters | | | | Removal efficiency ($\eta$, %) | | |
|---|---|---|---|---|---|---|
| Initial Concentration | pH | Dosage | Time | Predicted | Actual | Desirability |
| 18.747 | 2.770 | 0.048 | 85.884 | 98.878 | 97.98 | 0.987 |

**Table 6.** Textural properties of prepared $CoFe_2O_4$/ZnAl LDH adsorbent.

| Adsorbent | BET surface area $(m^2 g)^{-1}$ | pore volume (c.c./g) | pore diameter (nm) |
|---|---|---|---|
| $CoFe_2O_4$/ZnAl-LDH | 499.345 | 0.9321 | 1.27 |
| ZnAl-LDH | 524.6 | 1.139 | 5.27 |

**Table 7.** Adsorption kinetic constants and correlation coefficients of MO adsorption onto $CoFe_2O_4$/ZnAl-LDH composite.

| Model | Parameters | Values | $R^2$ |
|---|---|---|---|
| Pseudo-first-order | $q_{e,exper.}$ $(mg\,g)^{-1}$ | 19.753 | 0.9366 |
| | $q_{e,calc.}$ $(mg\,g)^{-1}$ | 3.241 | |
| | $K_1$ $(min^{-1})$ | 0.0277 | |
| Pseudo-second-order | $q_{e,calc.}$ $(mg\,g)^{-1}$ | 20.137 | 0.9998 |
| | $K_2$ $(min^{-1})$ | 0.01696 | |

500 rpm for 87 min and at room temperature was taken. The non-linear fitting results from the isotherms were listed in table 6. According to the values of $R^2$, the Langmuir model is more suitable than the Freundlich model to describe the adsorption of MO, indicating homogenous adsorption on magnetic $CoFe_2O_4$/ZnAl-LDH composite. Moreover, the values of $R_L$ was comprised within 0 to 1; confirm the favorability of Langmuir adsorption [42].

### 3.5.4. Adsorption kinetics
The kinetic parameters of the teo models were evaluted from the combined plots (figure 6) and the values of the parameters are summarized in table 7. From this table, The $R^2$ value of the pseudo-second order model was found to be higher than obtained from the pseudo-first order model. Therefore, the pseudo-second order model

precisely explains the adsorption of MO on the surface of the adsorbent, indicating that the rate-limiting step in adsorption process is probably the chemisorption [43].

### 3.5.5. Adsorption mechanism

The adsorption mechanism of MO could follow the following steps. First, Adsorption takes place at the surface of the $CoFe_2O_4$/ZnAl-LDH composite through electrostatic forces of attraction i.e., the negatively charged sulfonated group ($-SO_3^-Na^+$) on MO could be strongly attracted towards the positively charged $CoFe_2O_4$/ZnAl-LDH surface, followed by the interlayer $CO_3^{2-}$ anion, which was consequently replaced by $SO_3^-$ anion of MO via anion exchange [44], then the aromatic C=C and/or N=N enter into the structure of magnetic $CoFe_2O_4$/ZnAl-LDH composite.

## 4. Conclusion

Magnetic $CoFe_2O_4$/ZnAl-LDH composite was successfully prepared, well characterized by XRD, SEM, FTIR, and BET, and employed as an adsorbent for MO removal. Adsorption processes were performed as a function of independent process variables such as the initial MO concentration, PH, adsorbent dosage, and contact time using the RSM-CCD method. By adopting the design of experiments, statistically, it was optimized that the maximized removal (98.874%) of MO can be achieved via 18.747 mg l$^{-1}$ initial MO concentration, 2.770 solution pH, 0.048 g adsorbent dosage, and 85.890 min contact time. MO adsorption on CoFe2O4/ZnAl-LDH follows the pseudo-second-order and the Langmuir monolayer models. Electrostatic attraction and anion exchange are the main adsorption mechanisms.

## Acknowledgments

## Data availability statement

The data generated and/or analysed during the current study are not publicly available for legal/ethical reasons but are available from the corresponding author on reasonable request.

## ORCID iDs

Yiene Molla Desalegn ⓘ https://orcid.org/0000-0002-5475-2852
Temesgen Debelo Desissa ⓘ https://orcid.org/0000-0003-3612-7153

## References

[1] Sajjad T A and Al-zobai K M M 2020 Investigation the effect of intensity and direction of light on the removal of reactive blue dye from simulated wastewater using photo-Fenton oxidation under UV irradiation: batch and continuous methods *IOP Conference Series: Materials Science and Engineering* (IOP Publishing)

[2] Jia Z *et al* 2015 Synthesis of MgAl-LDH/CoFe$_2$O$_4$ and MgAl-CLDH/CoFe$_2$O$_4$ nanofibres for the removal of Congo red from aqueous solution *Bull. Mater. Sci.* **38** 1757–64

[3] Natarajan S *et al* 2020 Synthesis and characterization of magnetic superadsorbent Fe3O4-PEG-Mg-Al-LDH nanocomposites for ultrahigh removal of organic dyes *ACS Omega* **5** 3181–93

[4] Pawar R R *et al* 2018 Porous synthetic hectorite clay-alginate composite beads for effective adsorption of methylene blue dye from aqueous solution *International Journal of Biological Macromolecules* **114** 1315–24

[5] Hanafi M F and Sapawe N J M T P 2020 A review on the water problem associate with organic pollutants derived from phenol, methyl orange, and remazol brilliant blue dyes *Mater. Today* **31** A141–50

[6] Pirsaheba M *et al* 2019 Photocatalyzed degradation of acid orange 7 dye under Sunlight and ultraviolet irradiation using Ni-doped ZnO nanoparticles *Desalination and Water Treatment* **165** 321–32

[7] Pirsaheb M *et al* 2020 Optimization of photocatalytic degradation of methyl orange using immobilized scoria-Ni/TiO2 nanoparticles *Journal of Nanostructure in Chemistry* **10** 143–59

[8] Lei S *et al* 2020 Ultrathin dodecyl-sulfate-intercalated Mg-Al layered double hydroxide nanosheets with high adsorption capability for dye pollution *J. Colloid Interface Sci.* **577** 181–90

[9] Lin Z and Chen J J C 2021 Magnetic Fe$_3$O$_4$@ MgAl-LDH@ La (OH) 3 composites with a hierarchical core–shell structure for phosphate removal from wastewater and inhibition of labile sedimentary phosphorus release *Chemosphere* **264** 128551

[10] Desalegn Y M, Andoshe D M and Desissa T D J M R E 2020 Composite of bentonite/CoFe2O4/hydroxyapatite for adsorption of Pb (II) *Materials Research Express* **7** 115501

[11] Zheng G *et al* 2019 Space-confined effect one-pot synthesis of $\gamma$-AlO (OH)/MgAl-LDH heterostructures with excellent adsorption performance *Nanoscale Research Letters* **14** 1–12

[12] Sheng T *et al* 2019 Adsorption of phosphorus by using magnetic Mg-Al-, Zn-Al- and Mg-Fe-layered double hydroxides: comparison studies and adsorption mechanism *Environ. Sci. Pollut. Res. Int.* **26** 7102–14

[13] Jiang Z *et al* 2020 Low-temperature synthesis of carbonate-intercalated NixFe-layered double hydroxides for enhanced adsorption properties *Appl. Surf. Sci.* **531** 147281

[14] Lv Q *et al* 2020 Synthesis of magnetic biochar/carbonate intercalated Mg–Al layered double hydroxides for enhanced Cd (II) removal from aqueous solution *Desalination and Water Treatment* **207** 258–69

[15] Sun J *et al* 2018 Removal of Cu2+, Cd2 + and Pb2 + from aqueous solutions by magnetic alginate microsphere based on Fe3O4/MgAl-layered double hydroxide *J. Colloid Interface Sci.* **532** 474–84

[16] Hao M *et al* 2020 Highly efficient adsorption behavior and mechanism of Urea-Fe3O4@ LDH for triphenyl phosphate *Environ. Pollut.* **267** 114142

[17] Mrózek O *et al* 2019 Mg-Al-La LDH-MnFe$_2$O$_4$ hybrid material for facile removal of anionic dyes from aqueous solutions *Appl. Clay Sci.* **169** 1–9

[18] Palza H, Delgado K and Govan J J A C S 2019 Novel magnetic CoFe$_2$O$_4$/layered double hydroxide nanocomposites for recoverable anionic adsorbents for water treatment *Appl. Clay Sci.* **183** 105350

[19] Sun Q *et al* 2020 Biotemplated fabrication of a 3D hierarchical structure of magnetic ZnFe2O4/MgAl-LDH for efficient elimination of dye from water *J. Alloys Compd.* **829** 154552

[20] Wu X *et al* 2016 PEG-assisted hydrothermal synthesis of CoFe$_2$O$_4$ nanoparticles with enhanced selective adsorption properties for different dyes *Appl. Surf. Sci.* **389** 1003–11

[21] Elgiddawy N *et al* 2017 New approach for enhancing Chlorella vulgaris biomass recovery using ZnAl-layered double hydroxide nanosheets *Journal of Applied Phycology* **29** 1399–407

[22] Karri R R *et al* 2018 Optimization and modeling of methyl orange adsorption onto polyaniline nano-adsorbent through response surface methodology and differential evolution embedded neural network *Journal of Environmental Management* **223** 517–29

[23] Beyan S M *et al* 2022 A statistical modeling and optimization for Cr (VI) adsorption from aqueous media via teff straw-based activated carbon: isotherm, kinetics, and thermodynamic studies *Adsorption Science and Technology* **2022** 240–60

[24] Javanbakht V and Ghoreishi S M J A S 2017 and Technology Application of response surface methodology for optimization of lead removal from an aqueous solution by a novel superparamagnetic nanocomposite *Adsorption Science and Technology* **35** 241–60

[25] Jaseela P, Garvasis J and Joseph A J J O M L 2019 Selective adsorption of methylene blue (MB) dye from aqueous mixture of MB and methyl orange (MO) using mesoporous titania (TiO$_2$)–poly vinyl alcohol (PVA) nanocomposite *J. Mol. Liq.* **286** 110908

[26] Sani H A, Ahmad M B and Saleh T A 2016 Synthesis of zinc oxide/talc nanocomposite for enhanced lead adsorption from aqueous solutions *RSC Adv.* **6** 108819–27

[27] Walsh K *et al* 2020 Equilibrium data and its analysis with the freundlich model in the adsorption of arsenic(V) on granular ferric hydroxide *Sep. Purif. Technol.* **243** 116704

[28] Romero-González J *et al* 2006 Potential of agave lechuguilla biomass for Cr(III) removal from aqueous solutions: thermodynamic studies *Bioresour. Technol.* **97** 178–82

[29] Al-Ghouti M A and Da'ana D A 2020 Guidelines for the use and interpretation of adsorption isotherm models: a review *J. Hazard. Mater.* **393** 122383

[30] Yusuff A S J A W S 2018 Optimization of adsorption of Cr (VI) from aqueous solution by leucaena leucocephala seed shell activated carbon using design of experiment *Applied Water Science* **8** 1–11

[31] Kumar N *et al* 2017 Controlled synthesis of microsheets of ZnAl layered double hydroxides hexagonal nanoplates for efficient removal of Cr (VI) ions and anionic dye from water *Journal of Environmental Chemical Engineering* **5** 1718–31

[32] Saleh A, Sarı T A and Tuzen M 2016 Chitosan-modified vermiculite for As(III) adsorption from aqueous solution: equilibrium, thermodynamic and kinetic studies *J. Mol. Liq.* **219** 937–45

[33] Ho Y-S and McKay G 1999 Pseudo-second order model for sorption processes *Process Biochem.* **34** 451–65

[34] Xu H *et al* 2013 Removal of lead (II) and cadmium (II) from aqueous solutions using spent Agaricus bisporus *The Canadian Journal of Chemical Engineering* **91** 421–31

[35] Martínez M *et al* 2006 Removal of lead(II) and cadmium(II) from aqueous solutions using grape stalk waste *J. Hazard. Mater.* **133** 203–11

[36] Yuan X *et al* 2017 Photocatalytic Cr (VI) reduction by mixed metal oxide derived from ZnAl layered double hydroxide *Applied Clay Science* **143** 168–74

[37] Aragaw S G *et al* 2022 Synthesis of CuAl-layered double hydroxide/MgO2 nanocomposite catalyst for the degradation of organic dye under dark condition *Applied Water Science* **12** 1–12

[38] Zhou D *et al* 2011 Electrophoretic deposition of multiferroic BaTiO$_3$/CoFe$_2$O$_4$ bilayer films *Mater. Chem. Phys.* **127** 316–21

[39] Thang P D *et al* 2005 Spinel cobalt ferrite by complexometric synthesis *J. Magn. Magn. Mater.* **295** 251–6

[40] Nyaba L *et al* 2021 Magnetic Fe$_3$O$_4$@ Mg/Al-layered double hydroxide adsorbent for preconcentration of trace metals in water matrices *Sci. Rep.* **11** 1–15

[41] Gidado S M and Akanyeti İ J W 2020 Air,, and S. Pollution, comparison of remazol brilliant blue reactive adsorption on pristine and calcined ZnAl, MgAl, ZnMgAl Layeed Double Hydroxides *An International Journal of Environmental Pollution* **231** 1–18

[42] Shan R-r *et al* 2014 Magnetic Fe$_3$O$_4$/MgAl-LDH composite for effective removal of three red dyes from aqueous solution *Chem. Eng. J.* **252** 38–46

[43] Zaghloul A *et al* 2021 Characterization and application of MgAl layered double hydroxide for methyl orange removal from aqueous solution *Mater. Today* **37** 3793–7

[44] Juang R-S *et al* 2018 Synthesis of magnetic Fe$_3$O$_4$/activated carbon nanocomposites with high surface area as recoverable adsorbents *J. Taiwan Inst. Chem. Eng.* **90** 51–60